NUMERICAL ALGORITHMS FOR POLYENERGETIC DIGITAL BREAST TOMOSYNTHESIS RECONSTRUCTION

JULIANNE CHUNG*, JAMES G. NAGY†, AND IOANNIS SECHOPOULOS‡

Abstract. Digital tomosynthesis imaging is becoming increasingly significant in a variety of medical imaging applications. Tomosynthesis imaging involves the acquisition of a series of projection images over a limited angular range, which, after reconstruction, results in a pseudo-3D representation of the imaged object. The partial separation of features in the third dimension improves the visibility of lesions of interest by reducing the effect of the superimposition of tissues. In breast cancer imaging, tomosynthesis is a viable alternative to standard mammography; however, current algorithms for image reconstruction do not take into account the polyenergetic nature of the x-ray source beam entering the object. This results in inaccuracies in the reconstruction, making quantitative analysis challenging and allowing for beam hardening artifacts. In this paper, we develop a mathematical framework based on a polyenergetic model and develop statistically based iterative methods for digital tomosynthesis reconstruction for breast imaging. By applying our algorithms to simulated data, we illustrate the success of our methods in suppressing beam hardening artifacts, and thus improving the quality of the reconstruction.

Key words. digital tomosynthesis, iterative methods, beam hardening artifacts

AMS Subject Classifications: 65F22, 65F10, 49N45, 65K99

1. Introduction. Ever since Röntgen produced the first medical x-ray image of his wife's hand in 1895, projection radiography, or x-ray imaging, has made a significant impact in the field of medical imaging. For example, mammography has played a key role in the early detection of breast cancer, allowing doctors to prevent metastatic spread and decrease the number of deaths related to breast cancer. However, a severe limitation of these conventional x-ray systems is that only one 2-dimensional (2-D) projection image of a 3-dimensional (3-D) object is available from each scan. The projection images have a severe decrease in contrast of structures due to the superimposition of overlaying tissue. Specifically in breast imaging, a false negative diagnosis may be caused by breast cancer obscured by overlapping tissue, while superimposed normal tissues may appear to be a cancerous mass, resulting in a false positive diagnosis [28].

Tomosynthesis is a technique for inversely constructing slices of a 3-D object from a set of 2-D projection images. Though the idea of tomosynthesis is rooted in the theory of conventional geometric tomography, known since the 1930s, it was not until the late 1960s and early 1970s when researchers put these ideas into practice [14, 15]. However tomosynthesis suffered from issues of practical implementation, including insufficient imaging detectors and inadequate computing technology. The introduction of digital technology and electronic image acquisition in the mid to late 70s significantly improved the contrast and resolution capabilities, compared to classical screen-film conventional x-ray systems, revitalizing research in tomosynthesis. Unfortunately, there were still computational and algorithmic limitations, and by the late 70s, tomosynthesis took a "back-seat" to other imaging techniques such as computed

tomography (CT) and magnetic resonance imaging (MRI) [9].

Computed tomography allows the three-dimensional reconstruction of objects by obtaining a complete 360 degree rotation of projection data around the object. Though impressive in many respects, CT has its limitations. The time to complete a CT scan and the radiation dosage requirements for CT can become prohibitively large compared to standard x-ray imaging. Furthermore, certain regions of the body such as breast tissue can be difficult to reconstruct with CT, due to the similar densities of breast tissue compared to water [11]. CT is particularly challenging for breast imaging because the patient must be in the prone position during the scan. In addition to being difficult for mobility challenged individuals, this positioning makes it difficult to effectively image the chest wall and axilla area [18]. These undesirable properties of CT, along with recent advancements in digital technology, post-processing reconstruction algorithms and computational power, have motivated and reignited interest in tomosynthesis as a viable alternative to CT.

The basic idea underlying tomosynthesis is that multiple 2-D image projections of the object are taken at varying incident angles, and each 2-D image provides different information about the 3-D object. See Figure 1.1 for an illustration of a typical geometry for breast tomosynthesis imaging. From the limited set of 2-D projection images, reconstruction algorithms should be able to reconstruct any number of slices of the 3-D object. Sophisticated approaches used for 3-D CT reconstruction cannot be applied here because projections are only taken from a limited angular range, leaving entire regions of the frequency space un-sampled. The main challenge in tomosynthesis reconstruction is to remove the out-of-plane blur caused by the backprojection. Variants of the shift-and-add algorithm have been proposed for performing the deblurring operation, but another class of algorithms, which we will follow in this paper, includes iterative reconstruction algorithms that seek to minimize an appropriate cost function. See [9] and references therein for a survey of previous approaches.

(a) Front view   (b) Side view with X-ray tube at 0°
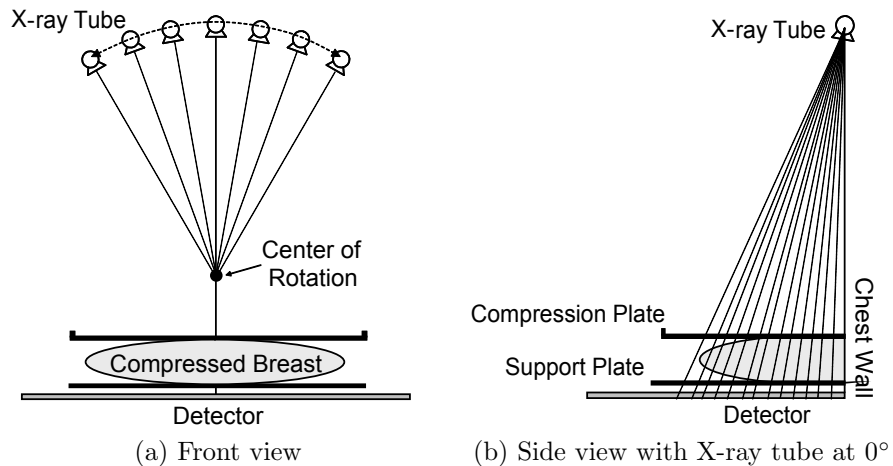
Fɪɢ. 1.1. *Typical geometry of the imaging device used in breast imaging.*

In this paper, we consider a statistical model for a Poisson random variable and investigate iterative optimization techniques for minimizing the resulting negative log likelihood function. Since the observed projection data from x-ray transmission tomography is known to follow a Poisson distribution, especially in the case of low-

count transmission scans, many researchers seek to maximize the corresponding log likelihood function. A common approach to solving the optimization problem uses a convexity argument to simplify the problem, a technique described in [21] and used for tomosynthesis reconstruction in [26, 27, 25, 28]. More recently, Chen and Barner [6] have proposed a multi-resolution, maximum a posteriori reconstruction algorithm, and Sidky et. al. [23] have implemented a total variation minimization algorithm.

However, an inaccurate assumption in nearly all of the previously proposed reconstruction algorithms is that the x-ray source is monoenergetic, that is, all incident photons have the same energy level. X-ray photons emitted from an x-ray tube have a distribution of energies, and as the x-ray beam passes through any attenuating medium (in this case the breast) there is a preferential absorption of low energy photons, resulting in an increase in the mean energy of the x-ray beam. This phenomenon, called *beam hardening*, is of concern in reconstruction methods developed for quantitative imaging because of the attenuation coefficients' important dependence on x-ray energy.

Ignoring this energy dependence in the mathematical model can lead to severe artifacts in the reconstructed image, apparent in "halo" effects around bones or streaking in the image. Specifically in breast imaging, "cupping" artifacts or background nonuniformities may appear and are evident in dark bands appearing behind dense objects or a reduction in overall contrast. Few researchers have studied methods for eliminating beam hardening artifacts, and then only in the case of x-ray computed tomography [1, 5, 7, 10, 11]. Previously proposed methods for eliminating beam hardening artifacts include preprocessing the projection data, post processing images, or utilizing a dual-energy imaging modality. All of these approaches have some limitations.

In this paper, we propose a new mathematical formulation that takes into account the polyenergetic source spectrum in order to eliminate beam hardening artifacts and allow for quantitative imaging. We develop a maximum likelihood framework in which standard optimization algorithms can be used for tomosynthesis reconstruction. The model we propose is specific to digital breast tomosynthesis but can be easily extended to other nonlinear tomographic imaging applications. Section 2 derives the mathematical framework for modeling the effect of polyenergetic x-rays on the observed images. In this section, we develop a statistical framework that results in a Poisson-based model cost function to minimize. Then in Section 3 we discuss some of the properties of the problem and consider a variety of optimization techniques for solving the inverse problem of reconstructing a 3-D image from 2-D projection images. Numerical results in Section 4 illustrate the success of our proposed algorithms, and conclusions and future directions can be found in Section 5.

2. Polyenergetic Tomosynthesis Model. In this section, we describe the image acquisition process for breast tomosynthesis and develop a statistical model for image reconstruction. In particular, we develop a mathematical model based on a polyenergetic x-ray source spectrum and derive a statistical model for the problem.

Although most x-ray projection models are derived in terms of the density values for the voxels, it is common in breast imaging to interpret the voxels as a composition of adipose tissue, glandular tissue, or a combination of both [16]. Thus, each voxel of the object can be represented using the percentage glandular fraction, i.e. the percentage of glandular tissue present in that voxel. If density or attenuation coefficient values are desired, then these can be obtained from the glandular fraction through a simple algebraic transformation.

2.1. Polyenergetic Model Development.   Assume that the 3D object is discretized into a regular grid of voxels, and that each of the 2D projection images is discretized into a regular grid of pixels. Specifically, let N represent the number of voxels in the discretized 3D object and M be the number of pixels in a discretized 2D projection image. In practice N is on the order of a few billion and M is the order of a few million, depending on the size of the imaging detector. The energy dependent linear attenuation coefficient for voxel $j = 1, 2, ..., N$ in the breast can be represented as

$$\mu(e)^{(j)} = s(e)g_{true}^{(j)} + z(e),$$

where $g_{true}^{(j)}$ represents the percentage glandular fraction in voxel j of the "true" object, and $s(e)$ and $z(e)$ are known energy-dependent linear fit coefficients. This type of decomposition to reduce the number of degrees of freedom is similar to an approach used by De Man et. al. [7] for CT, in which they express the energy dependent linear attenuation coefficient in terms of its photoelectric component and Compton scatter component. However, their model is not optimal for our particular application.

In tomosynthesis, a limited number of projections are taken from various angles in a predetermined angular range, and the photon energies are discretized into a fixed number of levels. Let there be n_θ angular projections and assume the incident x-ray has been discretized into n_e photon energy levels. In practice, a typical scan may have $n_\theta = 21$ and $n_e = 43$. We would like to formulate a mathematical representation for the θth projection image. For a particular projection angle, we first compute a monochromatic ray trace for energy e and then sum over all energies. Let $a^{(ij)}$ represent the length of the ray that passes through voxel j, contributing to pixel i. Then the discrete monochromatic ray trace for pixel i can be represented by

$$\sum_{j=1}^{N} \mu(e)^{(j)} a^{(ij)} = s(e) \sum_{j=1}^{N} g_{true}^{(j)} a^{(ij)} + z(e) \sum_{j=1}^{N} a^{(ij)}. \tag{2.1}$$

Using the standard mathematical model for transmission radiography, the ith pixel value for the θth noise-free projection image, incorporating all photon energies present in the incident x-ray spectrum, can be written as

$$b_\theta^{(i)} = \sum_{e=1}^{n_e} \varrho(e) \exp\left(-\sum_{j=1}^{N} \mu(e)^{(j)} a^{(ij)}\right), \tag{2.2}$$

where $\varrho(e)$ is a product of the current energy with the number of incident photons at that energy.

To simplify notation, let's define $\mathbf{A}_\theta$ to be an $M \times N$ matrix with entries $a^{(ij)}$. Then equation (2.1) is simply the ith entry of vector

$$s(e)\mathbf{A}_\theta \mathbf{g}_{true} + z(e)\mathbf{A}_\theta \mathbf{1},$$

where $\mathbf{g}_{true}$ is a vector whose j^{th} entry is $g_{true}^{(j)}$ and $\mathbf{1}$ is a vector of all ones. Furthermore, the θth noise-free projection image in vector form can be written as

$$\mathbf{b}_\theta = \sum_{e=1}^{n_e} \varrho(e) \exp\left(-[s(e)\mathbf{A}_\theta \mathbf{g}_{true} + z(e)\mathbf{A}_\theta \mathbf{1}]\right) \tag{2.3}$$

where the exponential function is applied component-wise.

Tomosynthesis reconstruction is an inverse problem where the goal is to approximate the volume $\mathbf{g}_{true}$, given the set of projection images from various angles, $\mathbf{b}_\theta$, $\theta = 1, 2, ...n_\theta$. In the next subsection, we discuss a statistically based model for solving this problem.

2.2. A Poisson Based Likelihood Function. It is widely accepted in the medical imaging community that measurements obtained by x-ray transmission imaging, i.e. photon counts, can be accurately modeled as independently distributed Poisson random variables, with additional background noise. Based on x-ray projection model (2.1) and (2.2), the expected value for the measured data at pixel i for angle θ given volume approximation $\mathbf{g}$ can be written as

$$E[b_\theta^{(i)}, \mathbf{g}] = \sum_{e=1}^{n_e} \varrho(e) \exp\left(-\left[s(e)\sum_{j=1}^{N} g^{(j)} a^{(ij)} + z(e)\sum_{j=1}^{N} a^{(ij)}\right]\right) + \bar{\eta}^{(i)} \quad (2.4)$$

$$= \bar{b}_\theta^{(i)} + \bar{\eta}^{(i)}, \quad (2.5)$$

where $\bar{\eta}^{(i)}$ represents errors due to electronic noise and scatter in the observed data. In tomography applications, it is assumed that the additive noise is a realization of a Poisson random variable, where the statistical mean $\bar{\eta}^{(i)}$ is known or can be approximated.

For each angle, the measured data can be statistically modeled as an independent Poisson random process [10]. That is, the ith pixel of the observed projection image, $\mathbf{b}_\theta$, is a realization of a Poisson random variable with mean, $\bar{b}_\theta^{(i)} + \bar{\eta}^{(i)}$:

$$b_\theta^{(i)} \sim \text{Poisson}(\bar{b}_\theta^{(i)} + \bar{\eta}^{(i)}).$$

Thus, we can say that the probability or likeliness of observing projection image $\mathbf{b}_\theta$, given volume $\mathbf{g}$, is described by the likelihood function [17, 24]

$$p(\mathbf{b}_\theta, \mathbf{g}) = \prod_{i=1}^{M} \frac{e^{-(\bar{b}_\theta^{(i)}+\bar{\eta}^{(i)})}(\bar{b}_\theta^{(i)} + \bar{\eta}^{(i)})^{b_\theta^{(i)}}}{b_\theta^{(i)}!}. \quad (2.6)$$

We would like to compute the glandular fractions $\mathbf{g}$ that maximize this likelihood function. For ease of computation, a monotonic negative log operation is applied to the likelihood function (2.6), and the maximum likelihood estimator (MLE) can be found by minimizing the negative log likelihood function

$$-L_\theta(\mathbf{g}) = -\log p(\mathbf{b}_\theta, \mathbf{g})$$

$$= \sum_{i=1}^{M} (\bar{b}_\theta^{(i)} + \bar{\eta}^{(i)}) - b_\theta^{(i)} \log(\bar{b}_\theta^{(i)} + \bar{\eta}^{(i)}) \quad (2.7)$$

for all θ. In the next section, we consider efficient algorithms for minimizing the above negative log likelihood function.

3. Iterative Reconstruction Algorithms. In this section, we describe some numerical algorithms for estimating the MLE solution for the polyenergetic tomosynthesis reconstruction problem

$$\mathbf{g}_{MLE} = \min_{\mathbf{g}} \left\{ \sum_{\theta=1}^{n_\theta} -L_\theta(\mathbf{g}) \right\}. \quad (3.1)$$

To simplify notation in the derivation, we fix a particular angle θ and drop the subscript for the remainder of this section.

For a monoenergetic likelihood function, a variety of researchers have studied this optimization problem. In 1995, Lange and Fessler [21] presented a comparison of the EM algorithm, a scaled gradient descent algorithm, and a "convex" algorithm, in which properties of convexity were used to iteratively approximate the log likelihood function [20, 12]. Under simplifying assumptions that the solution exists, is unique and lies in the interior of the feasible region, they prove that all three methods converge locally to the MLE solution. Furthermore, they prove global convergence for the EM and convex algorithm when applied to the log posterior function

$$\Phi(\mathbf{g}) = L(\mathbf{g}) - \lambda R(\mathbf{g}),$$

where $R(\mathbf{g})$ is a penalizing prior, or smoothing function, and λ is a regularization parameter controlling the accepted level of smoothness. By selecting a strictly convex prior function, strict concavity of the log posterior function can be established [21]. However, all of the derivations assume a monoenergetic x-ray source and a strictly convex cost function, meaning noise is set to zero in the model (c.f. [13] for derivation).

Our problem not only assumes a polyenergetic x-ray beam, but also takes into account the presence of noise in the data. Thus, the theories from these previous algorithms for maximizing the likelihood and posterior functions do not apply. More specifically, due to severe nonlinearities, our polyenergetic cost function may not be convex, and regularization must be incorporated to suppress the noise.

With respect to convexity, we derive some reasonable assumptions under which our polyenergetic cost function is convex. With the new formulation, it can be shown that the the cost function is convex with respect to the glandular fractions, under the following two conditions:

1. $\mathbf{A}$ is full rank, and
2. $b^{(i)} - (\bar{b}^{(i)} + \bar{\eta}^{(i)}) \leq \dfrac{\min_e s(e)}{\max_e s(e)} \left(\dfrac{b^{(i)}}{\bar{b}^{(i)} + \bar{\eta}^{(i)}} \right) \bar{b}^{(i)}$ for all i.

In our numerical experiments, we found that the first condition holds true, and a good initial guess that satisfies the second condition is not difficult to obtain.

In regards to the additive noise, selecting the optimal regularizing function $R(\mathbf{g})$ for breast tomosynthesis reconstruction is still an open question. It has been noted that for transmission image reconstruction, nonquadratic, edge-preserving penalty functions are more desirable for images with piecewise smooth regions [8, 13]. For the monoenergetic case, Bleuet et. al. [3] suggested an adaptive 3D regularization scheme, Sidky et. al. [23] and Kastanis et. al. [19] implemented a total variation optimization approach and Chen and Barner [6] use a Markov random fields regularization function. For the polyenergetic case, Elbakri and Fessler [11] used a convex, edge-preserving Huber penalty for its desirable properties. However, current research has not yet determined optimal regularization methods for breast image reconstruction, and this topic should be investigated in future studies. For this paper, we incorporate regularization to deal with noise and errors in the data via early termination of the iterations. That is, we focus on the new polyenergetic formulation and investigate optimization algorithms to minimize the original negative log likelihood function (2.7).

We consider a gradient descent and a Newton algorithm. To do this, we need to compute the gradient and Hessian of the objective function with respect to the 3-D

volume, $\mathbf{g}$. We first establish two important equalities:

$$\frac{\partial \bar{b}^{(i)}}{\partial g^{(j)}} = -a^{(ij)} \sum_{e=1}^{n_e} \varrho(e)s(e) \exp\left(-\left[s(e)\sum_{j=1}^{N} a^{(ij)}g^{(j)} + z(e)\sum_{j=1}^{N} a^{(ij)}\right]\right) \quad (3.2)$$

$$\frac{\partial}{\partial g^{(\ell)}}\left(\frac{\partial \bar{b}^{(i)}}{\partial g^{(j)}}\right) = a^{(i\ell)}a^{(ij)} \sum_{e=1}^{n_e} \varrho(e)s(e)^2 \exp\left(-\left[s(e)\sum_{j=1}^{N} a^{(ij)}g^{(j)} + z(e)\sum_{j=1}^{N} a^{(ij)}\right]\right)(3.3)$$

These equations will aid in the derivation of the following algorithms.

3.1. Gradient descent. The first approach we consider is a simple gradient descent algorithm for minimizing equation (2.7), which takes the following form

$$\mathbf{g}_{k+1} = \mathbf{g}_k - \alpha_k \nabla L(\mathbf{g}_k) \quad (3.4)$$

where α_k is an iteration dependent step length parameter and $\nabla L(\mathbf{g}_k) = \frac{\partial}{\partial g^{(j)}}(-L_\theta)$ for all θ.

The first derivative of the negative log likelihood function with respect to $\mathbf{g}$ is given by

$$\frac{\partial}{\partial g^{(j)}}(-L) = \sum_{i=1}^{M}\left(1 - \frac{b^{(i)}}{\bar{b}^{(i)} + \bar{\eta}^{(i)}}\right)\frac{\partial \bar{b}^{(i)}}{\partial g^{(j)}}$$

$$= \sum_{i=1}^{M} a^{(ij)}\left(\frac{b^{(i)}}{\bar{b}^{(i)} + \bar{\eta}^{(i)}} - 1\right)\sum_{e=1}^{n_e}\varrho(e)s(e)\exp\left(-\left[s(e)\sum_{j=1}^{N}a^{(ij)}g^{(j)} + z(e)\sum_{j=1}^{N}a^{(ij)}\right]\right)$$

where the second equation follows from equation (3.2). Using matrix notation, the gradient can be written simply as

$$\nabla L(\mathbf{g}_k) = \mathbf{A}^T \mathbf{v}$$

where $\mathbf{v}$ is a vector whose entries are

$$v^{(i)} = \left(\frac{b^{(i)}}{\bar{b}^{(i)} + \bar{\eta}^{(i)}} - 1\right)\sum_{e=1}^{n_e}\varrho(e)s(e)\exp\left(-\left[s(e)\sum_{j=1}^{N}a^{(ij)}g^{(j)} + z(e)\sum_{j=1}^{N}a^{(ij)}\right]\right).$$

The gradient descent approach is known to converge slowly, and the step length parameter ensures that the objective function decreases.

3.2. Newton approach. Another approach for minimizing the negative log likelihood function is to employ a Newton method. Newton methods are well known to have faster convergence properties; however, they are more sensitive than gradient descent methods to noise in the data and require the initial estimate to be a good enough approximation. Furthermore, the Hessian may be nontrivial or impossible to compute. One of our main contributions to this project was to make the Newton approach feasible. That is, with the new polyenergetic formulation, we were able to derive an analytical formula for the Hessian matrix using some detailed calculus and matrix algebra. A typical Newton iteration has the following form

$$\mathbf{g}_{k+1} = \mathbf{g}_k - \alpha_k \mathbf{H}_k^{-1} \nabla L(\mathbf{g}_k). \quad (3.5)$$

Here we derive a mathematical formula for the Hessian. For $j = 1, 2, ...N$ and $\ell = 1, 2, ...N$, the $j\ell^{th}$ entry of the Hessian matrix, $\mathbf{H}$, can be written as

$$h^{(j\ell)} = \frac{\partial}{\partial g^{(\ell)}} \left(\frac{\partial}{\partial g^{(j)}} (-L(\mathbf{g})) \right)$$

$$= \frac{\partial}{\partial g^{(\ell)}} \left(\sum_{i=1}^{M} \left(1 - \frac{b^{(i)}}{\bar{b}^{(i)} + \bar{\eta}^{(i)}} \right) \frac{\partial \bar{b}^{(i)}}{\partial g^{(j)}} \right)$$

$$= \sum_{i=1}^{M} \left\{ \left(1 - \frac{b^{(i)}}{\bar{b}^{(i)} + \bar{\eta}^{(i)}} \right) \frac{\partial}{\partial g^{(\ell)}} \left(\frac{\partial \bar{b}^{(i)}}{\partial g^{(j)}} \right) + \frac{\partial \bar{b}^{(i)}}{\partial g^{(j)}} \frac{\partial}{\partial g^{(\ell)}} \left(1 - \frac{b^{(i)}}{\bar{b}^{(i)} + \bar{\eta}^{(i)}} \right) \right\}, \quad (3.6)$$

where the last equality is just application of the product rule. The derivative in the first term can be evaluated by equation (3.3) and the derivative in the second term can be expanded to be

$$\frac{\partial}{\partial g^{(\ell)}} \left(1 - \frac{b^{(i)}}{\bar{b}^{(i)} + \bar{\eta}^{(i)}} \right) = \frac{b^{(i)}}{(\bar{b}^{(i)} + \bar{\eta}^{(i)})^2} \frac{\partial \bar{b}^{(i)}}{\partial g^{(\ell)}}. \quad (3.7)$$

Now, plugging in (3.2), (3.3) and (3.7) into (3.6), we get the following expression for the $j\ell^{th}$ entry of the Hessian matrix

$$h^{(j\ell)} = \sum_{i=1}^{M} a^{(ij)} a^{(i\ell)} \left\{ \left(1 - \frac{b^{(i)}}{\bar{b}^{(i)} + \bar{\eta}^{(i)}} \right) \sum_{e=1}^{n_e} \varrho(e) s(e)^2 \exp\left(- \left[s(e) \sum_{j=1}^{N} a^{(ij)} g^{(j)} + z(e) \sum_{j=1}^{N} a^{(ij)} \right] \right) \right.$$

$$\left. + \frac{b^{(i)}}{(\bar{b}^{(i)} + \bar{\eta}^{(i)})^2} \left[\sum_{e=1}^{n_e} \varrho(e) s(e) \exp\left(- \left[s(e) \sum_{j=1}^{N} a^{(ij)} g^{(j)} + z(e) \sum_{j=1}^{n^3} a^{(ij)} \right] \right) \right]^2 \right\}. \quad (3.8)$$

Since nothing in the curly brackets of equation (3.8) depends on j or ℓ, let's define vector $\mathbf{w}$ with entries

$$w^{(i)} = \{...\}, \quad (3.9)$$

then equation (3.8) simplifies to

$$h^{(j\ell)} = \sum_{i=1}^{M} a^{(ij)} a^{(il)} w^{(i)},$$

corresponding to the matrix

$$\mathbf{H} = \mathbf{A}^T \mathbf{W} \mathbf{A}$$

where $\mathbf{W}$ is a diagonal matrix with vector $\mathbf{w}$ on the diagonal. Note that only matrix $\mathbf{W}$ is iteration dependent. Thus,

$$\mathbf{H}_k = \mathbf{A}^T \mathbf{W}_k \mathbf{A},$$

and the Newton step at iteration k can be found by solving the following system:

$$\mathbf{H}_k \mathbf{s}_k = -\nabla L(\mathbf{g}_k). \quad (3.10)$$

Note that equation (3.10) is the normal equations formulation of the least squares problem

$$\min_{\mathbf{s}_k} \left\| \mathbf{W}_k^{\frac{1}{2}} \mathbf{A} \mathbf{s}_k - \mathbf{W}_k^{-\frac{1}{2}} \mathbf{v} \right\|_2 \quad (3.11)$$

where $\mathbf{W}_k^{\frac{1}{2}} = \mathrm{diag}(\mathbf{w}^{\frac{1}{2}})$. A variety of methods can be used to solve (3.11); in our work we use the conjugate gradient algorithm for least squares (CGLS) [2].

4. Numerical Examples. In this section, we illustrate the success of the proposed algorithms presented in Section 3 for solving the polyenergetic tomosynthesis reconstruction problem for a simulated breast imaging example.

Given a 3-D volume with $128 \times 128 \times 128$ voxels [4], we normalized the values so that the voxel values range between 0 and 100, each value representing the percentage fraction of glandular tissue in that voxel. Then 21 projection images were taken from equally spaced angles, within an angular range from $-30°$ to $30°$ at $3°$ intervals, using the typical geometry for breast tomosynthesis, illustrated in Figure 1.1. Each 2-D projection image was 192×256 pixels. The original object represented a medium-sized breast of size $12.8\,\text{cm} \times 12.8\,\text{cm} \times 6.4\,\text{cm}$, and the detector was $19.2\,\text{cm} \times 25.6\,\text{cm}$. The source to detector distance at $0°$ was set to 66 cm and the distance from the center of rotation to detector was 0 cm. The incident x-ray spectrum consisted of 43 different energy levels, from 5.0 keV to 26 keV, in 0.5 keV steps.

For each projection angle, the ray trace matrix $\mathbf{A}_\theta$ was computed using a cone beam model with Siddon's ray tracing algorithm [22]. For each of the reconstruction algorithms, we used an initial guess of the volume to be a uniform image with all voxel values set to 50, meaning half glandular and half adipose tissue. To simulate a more realistic example, we created the projection images using a $128 \times 128 \times 128$ volume, but reconstructed a $128 \times 128 \times 8$ volume. Furthermore, the projection images included enough additive Poisson noise so that the relative noise level was 0.1%. The slices of the volume that we would like to reconstruct can be found in Figure 4.1, and a few of the cropped, observed projection data can be found in Figure 4.2.
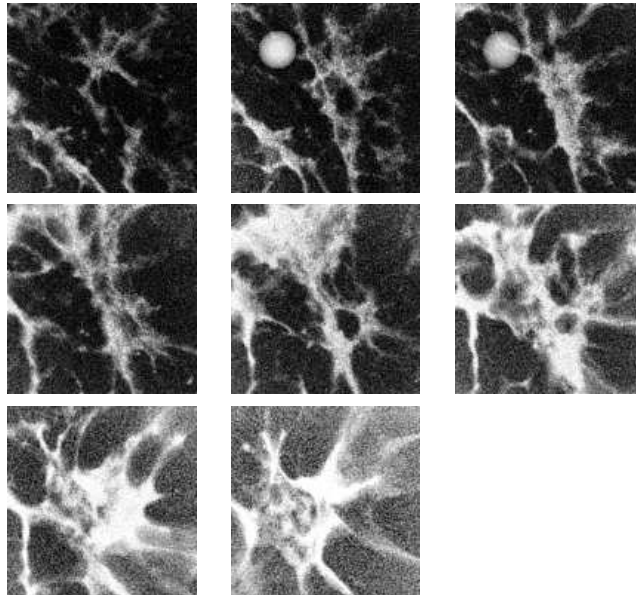
FIG. 4.1. *True volume slices.*

To evaluate the performance of each of the algorithms presented in Section 3, we present in Table 4.1 the relative objective function value, the relative gradient value and the relative error for the 3-D image. We note here that for the Newton algorithm, 50 iterations of the conjugate gradient algorithm were used to solve the inner problem in equation (3.11). Furthermore, in an application where the Hessian
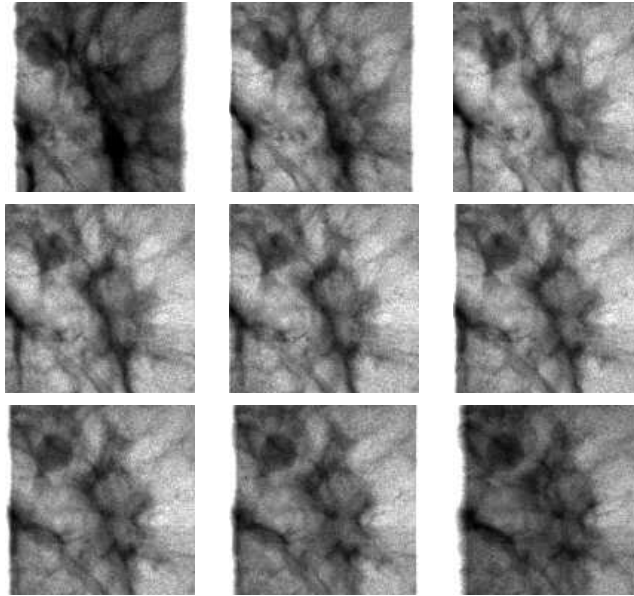
Fig. 4.2. *Sample Projection Images.*

Table 4.1
Convergence of iterations for polyenergetic tomosynthesis reconstruction.

Gradient Descent Method

iteration	relative objective	relative gradient	Image Error
0	1.739e-4	1.0000	0.6377
1	1.583e-4	0.6370	0.5994
25	1.440e-4	0.0349	0.4457
50	1.438e-4	0.0194	0.4189
75	1.436e-4	0.0314	0.3899
100	1.434e-4	0.0048	0.3107

Newton with CG

iteration	relative objective	relative gradient	Image Error
0	1.739e-4	1.0000	0.6377
1	1.499e-4	0.4120	0.4305
2	1.435e-4	0.0523	0.2838
3	1.433e-4	0.0035	0.2665
4	1.433e-4	0.0016	0.2731
5	1.433e-4	0.0010	0.2737

cannot be derived analytically, a Quasi-Newton approach such as LBFGS can be a good alternative. However, in our experience, the LBFGS method was quite slow in converging, and a Newton approach worked much better.

It is evident from Table 4.1 that 3 iterations of the Newton algorithm produced a small relative error for the image. However, without a comparison of timings or computational effort, it is difficult to present a fair comparison of the reconstruction algorithms. In Figure 4 we present a visual comparison of images, with slices

of the true volume in the first column. In the second column, we provide the "best" monoenergetic reconstruction of the linear attenuation coefficients using Lange and Fessler's "convex" algorithm. Recall that the monoenergetic algorithm reconstructs attenuation coefficients rather than glandular fractions, so by "best," we mean that this reconstruction provided the smallest computed image error between the reconstructed attenuation coefficients and the attenuation coefficients at the median energy level for the true volume. In the third and fourth columns, we present the images for gradient descent and Newton algorithms after approximately 30 minutes of wall clock time. In terms of timings, the Newton algorithm for this problem is the clear winner because it computed a solution with better visual quality.

It is important to remark here that with more iterations of the monoenergetic algorithm, the images become significantly worse in terms of contrast resolution. This is expected because we are using an inaccurate model for reconstruction. However, with more iterations of the gradient descent algorithm, the image will eventually resemble the superior quality obtained from Newton. Also, we remark that although the image errors in Table 4.1 decrease in early iterations, these errors will eventually increase. This is slightly evident in the later Newton iterations and is typical of ill-posed problems. Future work will be needed to develop methods to suppress noise amplification. From our numerical results, we have successfully shown that reconstruction based on a polyenergetic model can produce significantly better results than the current reconstruction algorithms.

5. Concluding Remarks. In this paper, we have described a novel formulation for polyenergetic tomosynthesis reconstruction and shown that standard numerical optimization techniques can be used to reconstruct 3-D volumes from limited angle 2-D projection images. Many researchers have studied the monoenergetic tomosynthesis problem, but few have investigated the nonlinear problem that arises from a polyenergetic spectrum. We have addressed this problem and shown that by reformulating the problem in terms of the glandular fractions, one can analytically compute the necessary gradients and Hessians for efficiently solving the nonlinear inverse problem.

Nonlinear inverse problems of this form arise in many applications, and we have focused on one particular application from breast imaging. Our numerical results illustrate the potential for successful application of sophisticated mathematical techniques and approaches to solve this problem. Future work includes efficient preconditioning for the inner iteration for the Newton algorithm. We also see potential benefits from implementing bound constrained algorithms to restrict the solution. Furthermore, a comprehensive evaluation of regularization methods for breast imaging needs to be investigated, as well as the development of accurate methods for selecting regularization parameters. A direction of particular interest from the medical community is the quantification of physical uncertainties from the system geometry. Due to the massive size and constant movement of the x-ray source, errors from misalignment of the x-ray tube with the image detector are inevitably introduced in the mathematical model. Efficient methods for estimating and correcting for these errors should be investigated. In addition, evaluating the performance of these methods in the presence of materials that do not conform to this model will be pursued in our future work.

	True	Best Mono(28)	Grad(50)	Newton(3)

Slice 1

Slice 2

Slice 3

Slice 4

Slice 5

Slice 6

Slice 7

Slice 8
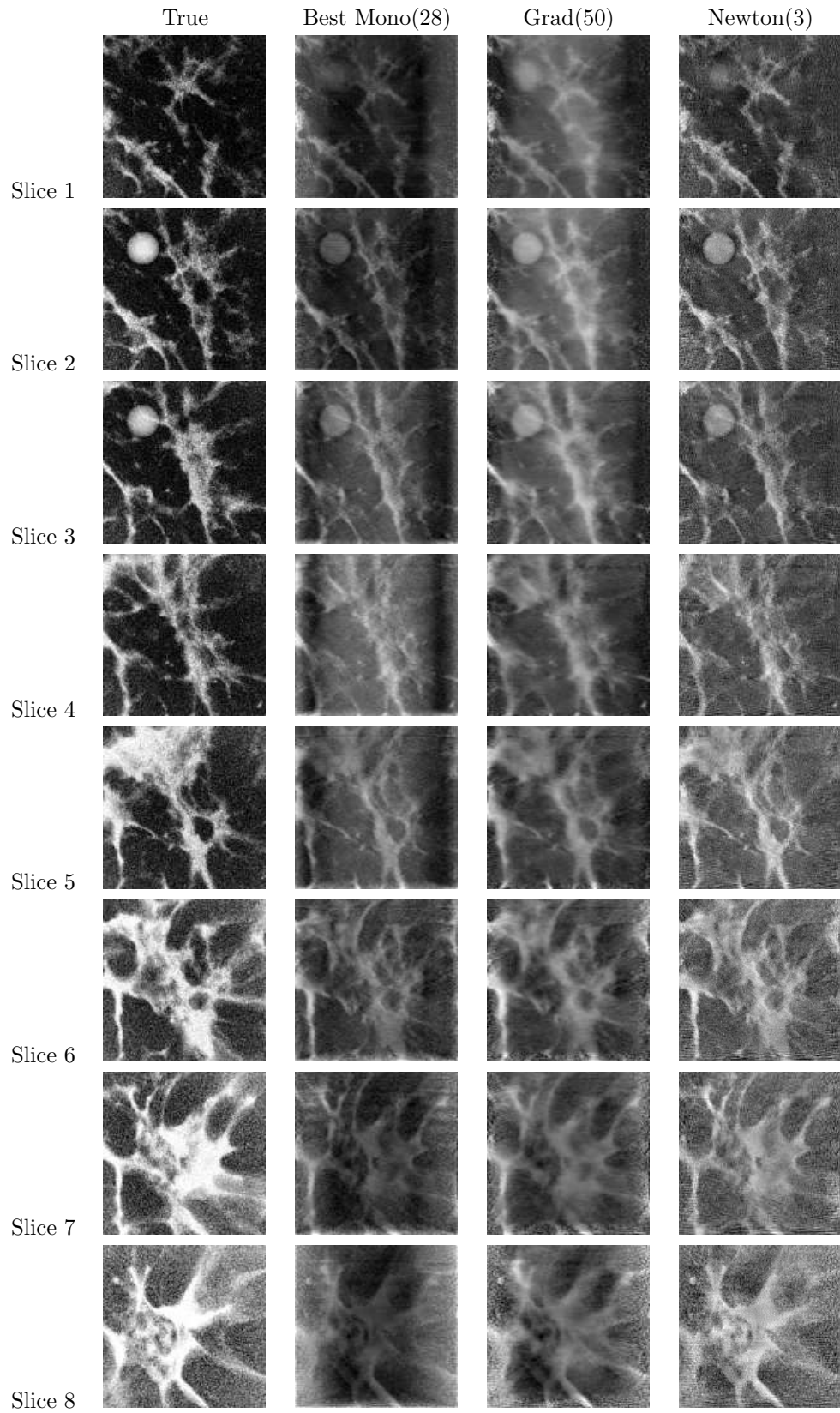
REFERENCES

[1] M. BAZALOVA, J. CARRIER, L. BEAULIEU, AND F. VERHAEGEN, *Dual-energy CT-based material extraction for tissue segmentation in Monte Carlo dose calculations*, Phys. Med. Biol., 53 (2008), pp. 2439–2456.

[2] Å. BJÖRCK, *Numerical Methods for Least Squares Problems*, SIAM, Philadelphia, PA, 1996.

[3] P. BLEUET, R. GUILLEMAUD, AND I. E. MAGNIN, *Resolution improvement in linear tomosynthesis with an adapted 3d regularization scheme*, Proc. SPIE, 4682 (2002), pp. 117–125.

[4] J. M. BOONE, T. R. NELSON, K. K. LINDFORS, AND J. A. SEIBERT, *Dedicated breast CT: Radiation dose and image quality evaluation*, Radiology, 221 (2001), pp. 657–667.

[5] R. BROOKS AND G. DI CHIRO, *Beam hardening in x-ray reconstructive tomography*, Phys. Med. Biol., 21 (1976), pp. 390–398.

[6] P. CHEN AND K. BARNER, *A multi-resolution statistical reconstruction for digital tomosynthesis*, Submitted to IEEE Trans. Med. Imaging, (2005). http://www.ece.udel.edu/∼pchen/My Publications/Tomo.pdf.

[7] B. DE MAN, J. NUYTS, P. DUPONT, G. MARCHAL, AND P. SUETENS, *An iterative maximum-likelihood polychromatic algorithm for CT*, IEEE Trans. Med. Imaging, 20 (2001), pp. 999–1008.

[8] A. H. DELANEY AND Y. BRESLER, *Globally convergent edge-preserving regularized reconstruction: An application to limited-angle tomography*, IEEE Trans. Image Process., 7 (1998), pp. 204–221.

[9] J. T. DOBBINS III AND D. J. GODFREY, *Digital x-ray tomosynthesis: current state of the art and clinical potential*, Phys. Med. Biol., 48 (2003), pp. R65–R106.

[10] I. A. ELBAKRI AND J. A. FESSLER, *Statistical image reconstruction for polyenergetic x-ray computed tomography*, IEEE Trans. Med. Imaging, 21 (2002), pp. 89–99.

[11] ———, *Segmentation-free statistical image reconstruction for polyenergetic x-ray computed tomography with experimental validation*, Phys. Med. Biol., 48 (2003), pp. 2453–2477.

[12] H. ERDOĞAN AND J. A. FESSLER, *Monotonic algorithms for transmission tomography*, IEEE Trans. Med. Imaging, 18 (1999), pp. 801–814.

[13] J. A. FESSLER, *Statistical image reconstruction methods for transmission tomography*, in Handbook of Medical Imaging, Medical Image Processing and Analysis, M. Sonka and J. M. Fitzpatrick, eds., vol. 2, SPIE, Bellingham, WA, 2000.

[14] J. B. GARRISON, D. G. GRANT, W. H. GUIER, AND R. J. JOHNS, *Three dimensional roentgenography*, Am. J. Roentgenol., 105 (1969), pp. 903–908.

[15] D. G. GRANT, *Tomosynthesis: A three-dimensional radiographic imaging technique*, IEEE Trans. Biomed. Eng., 19 (1972), pp. 20–28.

[16] G. R. HAMMERSTEIN, D. W. MILLER, D. R. WHITE, M. E. MASTERSON, H. Q. WOODARD, AND J. S. LAUGHLIN, *Absorbed radiation dose in mammography*, Radiology, 130 (1979), pp. 485–491.

[17] J. KAIPIO AND E. SOMERSALO, *Statistical and Computational Inverse Problems*, Springer, New York, 2005.

[18] A. KARELLAS, J. LO, AND C. ORTON, *Point/counterpoint: Cone beam x-ray CT will be superior to digital x-ray tomosynthesis in imaging the breast and delineating cancer*, Med. Phys., 35 (2008), pp. 409–411.

[19] I. KASTANIS, S. ARRIDGE, A. STEWART, S. GUNN, C. ULLBERG, AND T. FRANCKE, *3D digital breast tomosynthesis using total variation regularization*, in Lecture Notes in Computer Science, vol. 5116, Springer, 2008.

[20] K. LANGE, *An overview of bayesian methods in image reconstruction*, SPIE, 1351 (1990), pp. 270–287.

[21] K. LANGE AND J. A. FESSLER, *Globally convergent algorithms for maximum a posteriori transmission tomography*, IEEE Trans. Image Process., 4 (1995), pp. 1430–1438.

[22] R. L. SIDDON, *Fast calculation of the exact radiological path for a three-dimensional CT array*, Med. Phys., 12 (1985), pp. 252–255.

[23] E. Y. SIDKY, C. KAO, AND X. PAN, *Accurate image reconstruction from few-views and limited-angle data in divergent-beam CT*, Journal of X-Ray Science and Technology, 14 (2006), pp. 119–139.

[24] C. R. VOGEL, *Computational Methods for Inverse Problems*, SIAM, Philadelphia, PA, 2002.

[25] T. WU, R. H. MOORE, E. A. RAFFERTY, AND D. B. KOPANS, *A comparison of reconstruction algorithms for breast tomosynthesis*, Med. Phys., 31 (2004), pp. 2636–2647.

[26] T. WU, A. STEWART, M. STANTON, T. MCCAULEY, W. PHILLIPS, D. B. KOPANS, R. H. MOORE, J. W. EBERHARD, B. OPSAHL-ONG, L. NIKLASON, AND M. B. WILLIAMS, *Tomographic mammography using a limited number of low-dose cone-beam projection images*, Med.

Phys., 30 (2003), pp. 365–380.

[27] T. Wu, J. Zhang, R. Moore, E. Rafferty, D. Kopans, W. Meleis, and D. Kaeli, *Digital tomosynthesis mammography using a parallel maximum likelihood reconstruction model*, Proc. SPIE, 1 (2004), p. 5368.

[28] Y. Zhang, H. Chan, B. Sahiner, J. Wei, M. M. Goodsitt, L. M. Hadjiiski, J. Ge, and C. Zhou, *A comparative study of limited-angle cone-beam reconstruction methods for breast tomosynthesis*, Med. Phys., 33 (2006), pp. 3781–3795.